A Spatial Data Focusing and Generalized Time-invariant Frequency Diverse Array Approach for High Precision Range-angle-based Geocasting

Guylian Molineaux, *Student Member, IEEE,* François Horlin, *Member, IEEE,*
Philippe De Doncker, *Member, IEEE,* Julien Sarrazin, *Senior Member, IEEE*

***Abstract*—A novel unified frequency diverse array (FDA) and spatial data focusing (SDF) approach is proposed to simultaneously overcome time-variance and precision constraints of conventional FDA in geocasting, i.e., spatially confined broadcasting, scenarios. This paper describes a free space FDA-based SDF (FDA-SDF) system model for 2-dimensional range-angle-based focusing, including a generalized multi-purpose baseband approach for time-invariant FDA, complemented by SDF processing for improved spatial focusing precision and reduced array size. Comprehensive analytical derivations – general for any frequency offset configuration – describe the geographical FDA-SDF properties and design rules, such as geocast delivery zone steering, location, uniqueness, and size. Simulations of the proposed scheme validate theoretical derivations and demonstrate FDA-SDF's superior spatial precision and minimal design complexity. In particular, using novel alternating logarithmic frequency offsets, a 3-antenna FDA-SDF setup is shown to match the radial and azimuthal precision of its beamforming-based FDA counterpart using, respectively, 64 and 24 antennas.**

***Index Terms*—Geocasting, spatial data focusing (SDF), frequency diverse array (FDA), single-antenna multiple-channel (SAMC), time-invariance.**

I. Introduction

GEOCASTING, or location-based multicasting, aims to perform spatially confined broadcasting of information towards users within restricted geographic areas. It is an interesting technique in smart city and internet-of-things scenarios, where it can provide location-dependent services or messaging to large groups of mobile devices, e.g., for advertising and marketing, tourism, emergency signaling, traffic management, etc., [1], [2]. Moreover, by targeting a geographic area rather than individual users, it avoids potential privacy concerns as it requires no centralized knowledge of a user's location. While often achieved at the network layer by geographic routing algorithms [3], [4], these approaches require a challenging tradeoff between delivery rate, overhead, and scalability. Instead, by introducing spatial focusing capabilities at the base station, geocasting can be enforced at the physical layer. A geocast delivery zone is then generated where the bit error rate (BER) is sufficiently low.

Most evidently, beamforming can be exploited to realize the above scenario of physical-layer multicasting [5] or geocasting [6]. It performs spatial power focusing to manipulate the signal-to-noise ratio (SNR), and thereby the BER, to generate a geocast delivery zone. Notably, frequency diverse array (FDA) expands the foundation of classical phased array (PA) angular beamforming [7] to range-angle-dependent beamforming by varying each antenna's carrier frequency with small frequency offsets along the array. It originates from radar applications, pursuing joint angle and range estimation of targets [8] and providing range ambiguity resolution of pulsed transmissions [9]. Nevertheless, in continuous-wave transmission mode for communication scenarios, it enables range-angle-dependent interference suppression and user separation [10] – the latter being of significant interest for physical-layer geocasting. While original linear FDA [11] yields unbounded range-angle-coupled beampatterns that are unfit for geocasting, range-angle-decoupling of FDA beampatterns is enabled through nonlinear frequency offsets, such as logarithmic FDA [12], windowed FDA [13], random FDA [14]. However, FDA suffers – just as PA – from beamforming's inherent requirement for large physical arrays to generate narrow beams, thus inhibiting its achievable spatial precision for geocasting.

Inspired by directional modulation's (DM's) ability to secure beamforming communications in sidelobe directions, FDA has been most commonly investigated in physical-layer security (PLS) scenarios. In an attempt to exploit FDA's range-angle-dependent beamforming properties to extend angular domain secrecy of PA-DM [15] to both angle and range, numerous hybrid FDA-DM schemes have been proposed. Using artificial noise injection, both single-user [16], [17] as well as broadcasting [18] and multi-beam [19] FDA-DM variations have been investigated. Nevertheless, these approaches fail to overcome beamforming's large-scale array requirements, while often coming at the additional cost of increased design complexity. Moreover, recent work has revealed the commonly overlooked range-time-coupling and time-variance of FDA beampatterns [20] – an inherent

This work was supported by the ANR GEOHYPE project, grant ANR-16-CE25-0003 of the French Agence Nationale de la Recherche, and carried out in the framework of COST Action CA20120 INTERACT. G. Molineaux is a FRIA grantee of the Fonds de la Recherche Scientifique – FNRS.

G. Molineaux, F. Horlin, and P. De Doncker are with Université Libre de Bruxelles (ULB), OPERA – Wireless Communications Group, 1050 Brussels, Belgium. (e-mail: {gmolinea, fhorlin, pdedonck}@ulb.ac.be).

G. Molineaux and J. Sarrazin are with Sorbonne Université, CNRS, Laboratoire de Génie Electrique et Electronique de Paris, 75252 Paris, France and Université Paris-Saclay, CentraleSupélec, CNRS, Laboratoire de Génie Electrique et Electronique de Paris, 91192 Gif-sur-Yvette, France. (email: {guylian.molineaux, julien.sarrazin}@sorbonne-universite.fr).

physical limitation that is shown to inevitably jeopardize FDA's principal envisioned application of FDA-DM range-domain secrecy for PLS in wireless communications [21].

While the conclusions in [20] and [21] are indisputable, they consider only conventional FDA beamforming that relies on electromagnetic interference of transmitted signals at radio frequency (RF) for array radiation pattern manipulation, i.e., power focusing. Thus, they disregard the degree of freedom that is frequency down-conversion from RF to baseband, which – when applied individually on orthogonal signals transmitted from each antenna – allows to bypass FDA's time-variant RF interference, while preserving its range-angle-dependency. While also investigated for radars [22]–[24], this approach was explored for FDA-DM communications in [25], [26] through use of a single-antenna multiple-channel (SAMC) receiver. However, [22], [26] rely on band-pass or low-pass filtering for signal orthogonality, limiting frequency offset design, while [23]–[25] fail to account for multi-symbol transmission in their orthogonality criteria, undermining their validity for communications. Most importantly, [25], [26] – and derivated works – cannot restore PLS prospects for FDA as their inherent requirement for transmitter-receiver time-synchronization and dedicated receiver processing implies cooperative receivers that oppose PLS ambitions. Geocasting, on the other hand, can benefit from time-invariant FDA. However, current SAMC approaches are insufficiently adapted to this scenario due to their prior emphasis on PLS. Indeed, by attempting to mimic the FDA beamforming array factor in baseband, they inefficiently utilize orthogonal resources for the retransmission of identical information and, moreover, inherit its large-scale array requirements.

On the other hand, spatial data focusing (SDF) purposefully abandons power focusing ambitions and constraints to more efficiently address the geocasting use case [27]. In doing so, at the cost of sacrificing power efficiency, it unlocks an additional degree of freedom in its system design to improve spatial focusing precision. Specifically, it performs distributed transmission of information across an array, using uncorrelated and orthogonal signals. Dedicated equalization at cooperative geocasting receivers then exploits propagation differences between the datastreams from each antenna to induce a location-dependent symbol distortion that restricts the spatial accessibility of transmitted information. This novel approach allows SDF to increase focusing precision, reduce array size, and minimize design complexity compared to traditional beamforming-based approaches.
Time-based SDF (T-SDF) [28], which employs time resources for orthogonal signal transmission, has first demonstrated SDF's improved precision in the angular domain. By exploiting OFDM frequency resources, OFDM-based SDF (OFDM-SDF) has achieved high precision range-angle-based geocasting in both free space [29] and multipath [30] scenarios. Additionally, SDF's inherent inter-antenna signal orthogonality and independent substream processing make it naturally compatible with the SAMC receiver architecture to combat FDA time-variance, without increasing complexity over such approaches. In fact, similarly to [31], [32] in DM context, a time-invariant SAMC approach is used implicitly in OFDM-SDF through OFDM's orthogonal subcarrier nature. However, OFDM-SDF frequency offsets are restricted to OFDM subcarriers that lack the design flexibility of FDA for efficient manipulation of the geocast delivery zone.

By recognizing that time-invariant FDA requirements and its intrinsic geocasting operation are naturally met by SDF and its inherent SAMC-like receiver architecture, this paper proposes a hybrid FDA-based SDF (FDA-SDF) system in an attempt to shift ambition of FDA in wireless communications from PLS to geocasting. In doing so, it additionally combines SDF's high spatial precision with FDA's flexible frequency offset design for 2-dimensional range-angle-based geocasting. Preliminary work on FDA-SDF has been presented in [33]. However, in contrast to this work, its analysis is intuitive and lacks analytical description of the system's spatial properties. More specifically, this paper's main contribution is fourfold:

- *Generalized time-invariant FDA baseband system model.* 2-stage frequency up and down-conversion is introduced for flexible baseband modeling of FDA in wireless communications and universal time-invariant FDA orthogonality criteria are derived for arbitrary frequency offsets and filter waveforms.
- *Dedicated SDF precoding and cooperative geocasting receiver architecture.* It is shown that SDF distributed orthogonal transmission naturally complements time-invariant FDA requirements and simultaneously improves FDA focusing precision and SDF design flexibility.
- *Extensive analytical description of FDA-SDF's geographical behavior.* Correct symbol recovery conditions are derived to provide general, i.e., for arbitrary frequency offsets, design rules and descriptions for geocast delivery zone steering, location, uniqueness, and size.
- *Novel alternating logarithmic FDA frequency offsets.* By leveraging FDA-SDF's distinctive spatial features, they minimize azimuthal geocast delivery zone recurrence, guarantee its radial uniqueness, maximize azimuthal precision, and facilitate radial precision manipulation.

Section II introduces the proposed FDA-SDF system model, describing the time-invariant approach to FDA in Section II-A and complementary SDF processing in Section II-B. Geographical properties and design rules are derived in Section III. Simulations and performance analyses are performed in Section IV, leading to the conclusions in Section V.

II. System Model

Fig. 1 shows the proposed FDA-SDF system model. At the transmitter, it employs a uniform linear array of N antennas, with spacing b. Antennas are indexed by $n = -N_1, \dots, 0, \dots, N_2$, with $N_1, N_2 \in \mathbb{N}$, $N = N_1 + N_2 + 1$, and the origin is defined at antenna $n = 0$.[1] A single-antenna

[1]For simplicity, Fig. 1 shows only the common FDA setup with $n = 0, 1, \dots, N-1$. However, the subsequent discussion is valid for any type of FDA, regardless of the origin location in the array.

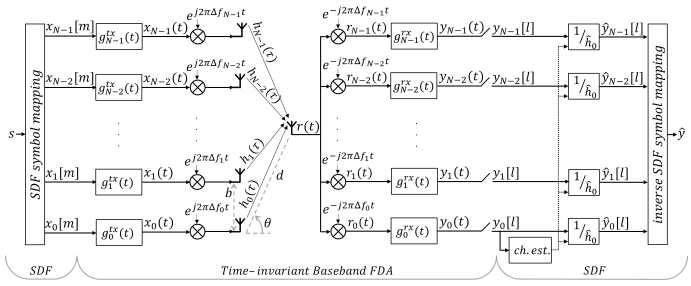

Fig. 1. FDA-based spatial data focusing baseband system model

receiver is considered and its position in the array plane is described by the polar coordinates (d, θ), with d the radial distance to the array origin and θ the azimuth angle with respect to the array broadside direction. The proposed model consists of distinct yet complementary FDA and SDF contributions. They are discussed individually below.

A. Time-invariant Baseband Frequency Diverse Array

As in conventional FDA, a specific carrier frequency f_n is allocated to each antenna n. They are defined by adding small frequency offsets Δf_n to a base carrier frequency f_c, i.e., $f_n = f_c + \Delta f_n$, with $\Delta f_n \ll f_c$. However, in contrast to a majority of conventional FDA literature that is limited in generality by embedding explicit frequency offset design rules in its models to capitalize on the distinct behavior they induce, this paper avoids any assumption or restriction on frequency offset assignment: the proposed approach is compatible with any arbitrary set of frequency offsets Δf_n.

1) Transmitter-side Signal Processing: At its input, each antenna n is fed with a stream of symbols $x_n[m]$, with symbol index $m \in \mathbb{N}$ and whose nature depends on the encompassing communication technique that incorporates the FDA, e.g., beamforming, DM, or SDF. The symbols $x_n[m]$ are then sequentially transmitted from each antenna through modulation of the transmitter waveforms $g_n^{tx}(t)$, with t the time variable. As such, the baseband signals $x_n(t)$ to be transmitted from each antenna n are given by

$$x_n(t) = \sum_m x_n[m] g_n^{tx}(t - mT_a), \tag{1}$$

where T_a is the array period, i.e., the time to transmit a symbol from each antenna in the array.

2) Baseband Frequency Diverse Array Channel Model: The proposed baseband FDA approach is characterized by a symmetric multi-frequency up and down-conversion, each performed in 2 stages. At the transmitter, each baseband signal $x_n(t)$ is first individually up-converted to an intermediate frequency (IF), corresponding to the frequency offset Δf_n assigned to their respective antennas. Collective up-conversion using the common base carrier frequency f_c then yields the appropriate radio frequency (RF) carrier $f_n = f_c + \Delta f_n$ for each antenna n. Reversely, the incoming RF signal at the receiver is first down-converted to IF using the common base carrier frequency f_c, after which down-conversion to baseband is performed separately by each of the frequency offsets Δf_n. As shown in Section II-A3, this multi-frequency down-conversion at the receiver is crucial in mitigating FDA time-variance. Additionally, given that $\Delta f_n \ll f_c$ for FDA, the 2-stage frequency up and down-conversion enables digital baseband-IF conversions. Although this increases the receiver's computational load, it reduces RF hardware complexity and increases practical frequency offset configuration flexibility compared to existing SAMC FDA literature [25], [26], and allows to model the RF propagation channel by the baseband channel impulse response (CIR), as described below.

In the above scenario, after up-conversion by the frequency offsets Δf_n, the corresponding IF signals transmitted from each antenna n become $x_n(t)e^{j2\pi\Delta f_n t}$. In free space, their respective propagation channels are characterized by distinct propagation delays τ_n, while an identical complex channel amplitude α can be assumed, considering close antenna spacing in the array.[2] Therefore, the baseband CIR $h_n(\tau)$ that models the RF propagation channel at the common base carrier frequency f_c for the n-th antenna is given by

$$h_n(\tau) = \alpha\delta(\tau - \tau_n)e^{-j2\pi f_c \tau_n}, \tag{2}$$

where τ is the delay variable and $\delta(\cdot)$ the Dirac delta function. The received baseband signals $r_v(t)$, after separate down-conversion of the aggregated received IF signal by the respective frequency offsets Δf_v, can then be written as

$$r_v(t) = \Big[\sum_n \big(x_n(t)e^{j2\pi\Delta f_n t}\big) * h_n(\tau) + z(t)\Big] e^{-j2\pi\Delta f_v t} \tag{3a}$$

$$= \Big[\sum_n \alpha x_n(t-\tau_n) e^{j2\pi\Delta f_n (t-\tau_n)} \times e^{-j2\pi f_c\tau_n} + z(t)\Big] e^{-j2\pi\Delta f_v t} \tag{3b}$$

$$= \sum_n \alpha x_n(t-\tau_n) e^{-j2\pi f_n\tau_n} e^{j2\pi\Delta f_{nv} t} + z_v(t), \tag{3c}$$

where $*$ is the convolution operator, $z(t) \sim \mathcal{CN}(0, \sigma_z^2)$ represents complex additive white Gaussian noise (AWGN) with variance σ_z^2, $z_v(t)$ is the noise after frequency down-conversion by Δf_v, and $\Delta f_{nv} = \Delta f_n - \Delta f_v = f_n - f_v$ is the difference between the up and down-conversion frequency offsets. Note that carrier phase offsets are omitted in (3a) under the assumption of transmitter-receiver synchronization to a common time reference – achievable in practice through satellite navigation systems such as GPS on-board clock or time-of-flight estimation. As anticipated, this implies cooperative receivers for time-invariant FDA – no different from SAMC FDA architectures like [25], [26] – and hence a geocasting scenario, ideally suited for SDF operation.

[2]While it is beyond the scope of this paper, an extended multipath channel model can easily be adopted for FDA-SDF analogous to the multipath OFDM-SDF model [30], assuming a line-of-sight channel component is guaranteed.

3) Receiver-side Signal Processing: In the received signal (3c) from the v-th receiver branch, while FDA's characteristic signal phases $e^{-j2\pi f_n \tau_n}$ and hence tractable range-angle-dependent inter-antenna phase differences are preserved, FDA's inherent time-variance is manifested through the presence of the time-variant phases $e^{j2\pi\Delta f_{nv} t}$. However, after individual down-conversion by the frequency offsets Δf_v, they affect only the signal components $x_n(t)$, $n \neq v$, as $\Delta f_{nv} = 0$ for identical up and down-conversion frequency offsets. As such, multi-frequency down-conversion ensures that each transmitted FDA signal component $x_v(t)$ remains time-invariant in the respective v-th receiver branch. In contrast to RF FDA models, demodulation then provides an additional degree of freedom in the proposed baseband approach to isolate and process time-invariant signal components. In particular, the signals $r_v(t)$ are demodulated through convolution with the receiver waveforms $g_v^{rx}(t)$, such that the demodulated signal $y_v(t)$ in the v-th receiver branch is given by

$$\begin{aligned} y_v(t) &= r_v(t) * g_v^{rx}(t) && \text{(4a)} \\ &= \sum_n \alpha e^{-j2\pi f_n \tau_n} \Bigg\{ \sum_m x_n[m] \\ &\quad \times \Big[\big(g_n^{tx}(t - \tau_n - mT_a) e^{j2\pi\Delta f_{nv} t} \big) * g_v^{rx}(t) \Big] \Bigg\} && \text{(4b)} \\ &\quad + z'_v(t), \end{aligned}$$

where $z'_v(t)$ is the demodulated noise.

After demodulation, the signal $y_v(t)$ is sampled according to the array period, i.e., $t = \tau_0 + lT_a$, to extract the v-th symbol stream's l-th received symbol $y_v[l]$. It is free from inter-symbol interference only when the transmitter and receiver waveforms, $g_n^{tx}(t)$ and $g_v^{rx}(t)$, ensure inter and intra-antenna signal orthogonality, despite the time-variant phases $e^{j2\pi\Delta f_{nv} t}$ affecting their convolution in (4b). Upon sampling, this results in the following orthogonality criterion for the transmitter and receiver waveforms

$$\int_{-\infty}^{+\infty} g_n^{tx}(\tau') g_v^{rx}\big((l-m)T_a - \tau'\big) e^{j2\pi\Delta f_{nv}\tau'} d\tau' = \delta_{nv}\delta_{ml}, \quad (5)$$

where δ_{ij} is the Kronecker delta function for integers i and j and a narrowband scenario, i.e., $|\tau_n - \tau_0| \ll T_a$, was assumed such that sampling offsets due to inter-antenna delay differences are negligible. Multiple waveforms may satisfy this requirement; in the context of FDA-SDF, a simple matched filtering approach is proposed in Section II-B. The l-th received symbol from the v-th symbol stream is then given by

$$y_v[l] = \alpha x_v[l] e^{-j2\pi f_v \tau_v} + z'_v[l], \quad (6)$$

where $z'_v[l]$ is the sampled noise. Thus, the multi-frequency down-conversion in the proposed baseband FDA approach allows to extract at each receiver branch v the symbols transmitted from the corresponding v-th FDA antenna, affected by the desired time-invariant FDA phase shift. Further processing can then be performed at will, according to the communication scheme that incorporates the FDA.[3]

B. Spatial Data Focusing

1) Transmitter-side Precoding: SDF employs distributed and orthogonal transmission of information from different antennas in an array to enforce its geocasting features. Therefore, for proper FDA-SDF operation, the FDA transmitter-side processing from Section II-A1 is preceded by appropriate SDF precoding. In particular, an arbitrary symbol stream s is first remapped to N symbol substreams s_n, assigned to each corresponding antenna n. Symbol mapping should be disjoint and exhaustive, so as to ensure that each substream carries unique yet complemental segments of the initial symbol stream. In this paper, for clarity and simplicity, this is achieved through simple alternating and cyclic mapping of successive symbols from s to the different substreams s_n, i.e., $s_n[m] = s[mN + n]$. Each substream is then transmitted from its respective antenna in the FDA. Specifically, the FDA input symbols $x_n[m]$ transmitted from the n-th FDA antenna in (1) carry the information in the corresponding SDF substream symbols $s_n[m]$, i.e.,

$$x_n[m] = s_n[m] e^{j\varphi_n^{steer}} = s[mN + n] e^{j\varphi_n^{steer}}. \quad (7)$$

The steering phase φ_n^{steer} is introduced to allow geocast delivery zone steering towards arbitrary target locations, as described in Section III-A.

The symbols $x_n[m]$ are then further processed as described by the FDA model in Section II-A. For the sake of simplicity, time-shifted orthogonal waveforms $g_n^{tx}(t) = g(t - nT)$, with $T = 1/B$ the symbol period for a symbol rate B, are adopted as the shaping pulses in the transmitted FDA signals (1), with a rectangular filter shape given by

$$g(t) = \begin{cases} 1/\sqrt{T} & |t| < T/2 \\ 0 & |t| \geq T/2. \end{cases} \quad (8)$$

The array period in (1) then becomes $T_a = NT$, such that the symbols $s_n[m]$ are time-sequenced in accordance to the SDF symbol mapping. Thus, SDF distributed transmission better complements time-invariant FDA inter-antenna orthogonality requirements than SAMC FDA architectures, e.g., [25], [26] that inefficiently utilize orthogonal and frequency resources for the retransmission of symbols carrying identical information. As such, just as conventional FDA, their spectral efficiency is reduced with respect to FDA-SDF by a factor equal to the number of antennas N.[4]

[3] As a single symbol with index $m = l$ from antenna $n = v$ is extracted upon sampling, the symbol index m and antenna index n unambiguously identify both the transmitted and received symbols. Therefore, without loss of generality, the indices l and v can be omitted in the remainder of this paper.

[4] Note that the time orthogonality in this work additionally avoids restrictions on the frequency offset configuration. As opposed to prior SDF [29], [30] and SAMC FDA-DM [26] schemes that exploit frequency orthogonality.

2) Receiver-side Channel Estimation & Equalization: Given the transmitter shaping pulse (8), orthogonality between the different received FDA signals in (4b) is ensured for FDA-SDF by adopting the transmitter pulse's matched filter as the FDA receiver shaping pulse, i.e., $g_n^{rx}(t) = g_n^{tx^*}(-t) = g^*(-t - nT)$. After the FDA receiver-side processing from Section II-A3, cooperative SDF geocasting receivers can then readily exploit the time-invariant FDA phase shift on the received symbols (6). As in [28]–[30], SDF performs channel estimation exclusively for a designated reference channel. For FDA-SDF in particular, the reference channel is defined to correspond to the reference antenna $n = 0$ at the FDA origin. It is estimated through traditional single-input single-output (SISO) transmission of an unsteered preamble. Equalization of the received symbols (6) from all antennas n is then performed using the same unique reference channel estimation.[5]

The following notations are introduced to interpret this equalization process. By assuming – without loss of generality – that the reference antenna's carrier frequency f_0 is equal to the base carrier frequency f_c, the frequency difference between the n-th channel and the reference is given by $\Delta f_n = f_n - f_c = f_n - f_0$. Similarly, the delay difference between the n-th channel and the reference is denoted as $\Delta\tau_n = \tau_n - \tau_0$. With these conventions, simple zero forcing [34] (i.e., multiplication with the inverted reference channel estimation) yields that the received equalized symbols from the n-th channel in FDA-SDF are given by

$$\hat{y}_n[m] = s_n[m]e^{j\varphi_n^{steer}}e^{-j2\pi f_0\Delta\tau_n}e^{-j2\pi\Delta f_n\tau_n} + \hat{z}_n[m], \quad (9)$$

where $\hat{z}_n[m]$ is the equalized noise sample. Thus, after dedicated SDF channel estimation and equalization, exploiting the FDA inter-antenna frequency offsets Δf_n and delay differences $\Delta\tau_n$, a residual phase shift is imposed on the received symbols (9), unique for the symbol substream from each antenna n. Its geographical properties, enabling geocasting functionality, are described in Section III. The complete symbol stream $\hat{y}$ is ultimately reconstructed at the receiver by inverting the transmitter-side symbol mapping, i.e., $\hat{y}[mN+n] = \hat{y}_n[m]$.

III. Geographical Properties & Design Rules

Undistorted recovery of the FDA-SDF received symbols (9) occurs only when their residual phase shift is an integer multiple of 2π, i.e.,

$$\varphi_n^{steer} - 2\pi f_0\Delta\tau_n - 2\pi\Delta f_n\tau_n = k_n 2\pi, \quad k_n \in \mathbb{Z}. \quad (10)$$

Under paraxial approximation ($b \ll d$), the delay τ_n and delay difference $\Delta\tau_n$ depend on the receiver position (d, θ):

$$\tau_n = \frac{d}{c} - n\frac{b}{c}\sin\theta, \quad (11a)$$

$$\Delta\tau_n = -n\frac{b}{c}\sin\theta, \quad (11b)$$

where c is the speed of light. Therefore, compliance to the residual phase condition (10) exhibits a tractable dependency on the receiver angle and range that can be leveraged to describe FDA-SDF's range-angle-based geocasting properties.

[5]Note that FDA-SDF channel estimation and equalization thus impose no additional cost compared to classical SISO communications.

A. Steering Phases

The steering phases φ_n^{steer}, added to the transmitted symbols (7) of their respective antennas, allow to enforce compliance to the residual phase condition (10) and hence correct data retrieval at an arbitrary geocasting target location $(d^{steer}, \theta^{steer})$. After isolating the steering phase φ_n^{steer} from (10), its final definition is found by evaluating (11a) and (11b) at the target coordinates $(d^{steer}, \theta^{steer})$ and substituting them for τ_n and $\Delta\tau_n$, while omitting the integer k_n as it modifies the steering phase by multiples of 2π only. One finds

$$\varphi_n^{steer} = 2\pi\left[\Delta f_n\frac{d^{steer}}{c} - f_n\frac{nb}{c}\sin\theta^{steer}\right]. \quad (12)$$

B. Geocast Delivery Zone Location(s)

Inserting the steering phase expression (12) and replacing τ_n and $\Delta\tau_n$ by their theoretical counterparts (11a) and (11b) in the residual phase condition (10), reveals its spatial dependency and allows to determine the coordinates (d_n, θ_n), where information transmitted from each non-reference antenna $n \neq 0$ is perfectly received. One finds

$$d_n(\theta) \approx d^{steer} + \frac{nb}{\lambda_0}\frac{c}{\Delta f_n}\left[\sin\theta - \sin\theta^{steer}\right] - \frac{c}{\Delta f_n}k_n, \quad (13a)$$

$$\sin\theta_n(d) \approx \sin\theta^{steer} + \frac{\lambda_0}{nb}\frac{\Delta f_n}{c}\left[d - d^{steer}\right] + \frac{\lambda_0}{nb}k_n, \quad (13b)$$

where it was noted that, by design, FDA frequency offsets satisfy $\Delta f_n \ll f_c = f_0$, such that $\frac{f_n}{c} \approx \frac{f_0}{c} = \frac{1}{\lambda_0}$, with λ_0 the reference antenna's carrier wavelength. The expressions (13a) and (13b) are equivalent, describing the same spatial pattern, and reveal that the region of correct retrieval of the n-th antenna's symbol substream follows a linear relation in the $(d, \sin\theta)$-plane that is periodic with a period of $\frac{c}{|\Delta f_n|}$ and $\frac{\lambda_0}{|n|b}$ along, respectively, the d and $\sin\theta$-axis.

Perfect retrieval of the complete transmitted symbol stream is achieved exclusively at the geographical location where the residual phase condition (10) is satisfied for all antennas n simultaneously. This occurs at the coordinates where the curves (13a) (equivalently (13b)) of perfect data recovery intersect for all non-reference antennas $n \neq 0$, i.e.,

$$\begin{aligned} d_{-N_1}(\theta) = \cdots = & d_{-1}(\theta) \\ & = d_1(\theta) = \cdots = d_{N_2}(\theta), \end{aligned} \quad (14a)$$

$$\begin{aligned} \sin\theta_{-N_1}(d) = \cdots = & \sin\theta_{-1}(d) \\ & = \sin\theta_1(d) = \cdots = \sin\theta_{N_2}(d). \end{aligned} \quad (14b)$$

Around these positions, the equalized symbols (9) from all antennas n are received with collectively negligible residual phase shifts, generating a spatially confined region of sub-threshold BER where transmitted information is exclusively retrievable, i.e., the geocast delivery zone. The exact geocast delivery zone location(s) are found as the solution(s) to

the above systems of $N-2$ equations. For $N \geq 4$, they are solved through mathematical induction.[6] First, as the induction step, the spatial periodicity of any arbitrary solution is studied. Next, as the induction base, the solutions within a single spatial period (the base case) are identified. From the latter, the complete set of solutions is found by applying the periodicity properties derived in the former.

1) Periodicity of Geocast Delivery Zone(s):

a) Radial periodicity: Considering that the residual phase condition solutions (13a) have a distinct radial periodicity $\frac{c}{|\Delta f_n|}$ for each antenna n, any intersection of these curves, i.e., solution to (14a) and (14b), can only appear at ranges coinciding with the curve (13a) of the antenna having the largest radial periodicity. To this end, $\tilde{n}$ is defined as the antenna index to which the smallest nonzero frequency offset in absolute value is allocated, i.e., $\Delta f_{\tilde{n}} = \arg\min_{\Delta f_n} \{|\Delta f_n|,\ n \neq 0,\ \Delta f_n \neq 0\}$, and thus manifesting the largest radial periodicity in (13a).

Given an arbitrary geocast delivery zone around coordinates (d^{sol}, θ^{sol}) as solution to (14a) and (14b), then the former imposes that $d_{\tilde{n}}(\theta^{sol}) = d_n(\theta^{sol}),\ \forall n \neq 0, \tilde{n}$. Further development of this statement, after inserting (13a) for antennas $\tilde{n}$ and n, yields

$$\frac{k_n}{\Delta f_n} - \frac{k_{\tilde{n}}}{\Delta f_{\tilde{n}}} = \Big(\frac{n}{\Delta f_n} - \frac{\tilde{n}}{\Delta f_{\tilde{n}}}\Big)\frac{b}{\lambda_0}\big[\sin\theta^{sol} - \sin\theta^{steer}\big]. \tag{15}$$

A radial recurrence of this solution exists only if the above statement is satisfied for a second pair of integers k'_n and $k'_{\tilde{n}}$. Noting that the right-hand side of (15) is invariant to the value of the integers k_n, $k_{\tilde{n}}$, k'_n, and $k'_{\tilde{n}}$, this occurs only when $\frac{k_n}{\Delta f_n} - \frac{k_{\tilde{n}}}{\Delta f_{\tilde{n}}} = \frac{k'_n}{\Delta f_n} - \frac{k'_{\tilde{n}}}{\Delta f_{\tilde{n}}}$ is satisfied. By writing $k'_{\tilde{n}} = k_{\tilde{n}} \pm q$ and $k'_n = k_n + p_n$, with $q \in \mathbb{Z}_0^+,\ p_n \in \mathbb{Z}_0$, one finds that radial recurrences of a geocast delivery zone appear only for frequency offsets satisfying $\Delta f_n = \pm\frac{p_n}{q}\Delta f_{\tilde{n}}$. Substitution of these results in (13a) reveals that the corresponding solution to (14a) and (14b) is given by the coordinates $(d^{sol} \mp q\frac{c}{\Delta f_{\tilde{n}}}, \sin\theta^{sol})$ in the $(d, \sin\theta)$-plane. The following property is so proven.

Property 1 (Radial Periodicity)**.** *Radial recurrences of an FDA-SDF geocast delivery zone exist only for frequency offsets $\Delta f_n = \frac{p_n}{q}\Delta f_{\tilde{n}},\ \frac{p_n}{q} \in \mathbb{Q}$ that can be written as rational multiples of the smallest nonzero frequency offset in absolute value $\Delta f_{\tilde{n}}$, with least common denominator $q \in \mathbb{Z}_0^+$. They are periodic with periodicity $T_d = q\frac{c}{|\Delta f_{\tilde{n}}|}$ along the d-axis.*
An FDA-SDF geocast delivery zone is unique in the radial domain when at least one frequency offset Δf_n is an irrational multiple of the smallest nonzero frequency offset in absolute value $\Delta f_{\tilde{n}}$, i.e., $\exists n\colon \Delta f_n = \rho_n \Delta f_{\tilde{n}},\ \rho_n \in \mathbb{R} \setminus \mathbb{Q}$.[7]

[6]The constraint $N \geq 4$ on the number of antennas is avoided when employing multiple frequency offsets per antenna. Curves (13a) and (13b) then exist for each frequency offset, rather than each antenna. Given at least 4 frequency offsets, the following discussion and results are identical and remain valid, such that there is no loss of generality in the presented approach.

[7]In the remainder of this paper, these two distinct categories of frequency offset configurations are referred to as rational frequency offsets and irrational frequency offsets, respectively.

b) Angular periodicity: Similarly to the radial dimension, the residual phase shift condition solutions (13b) have a distinct periodicity $\frac{\lambda_0}{|n|b}$ in the $\sin\theta$ dimension for each antenna n. As such, any intersection of these curves, i.e., solution to (14a) and (14b), can occur only at angles that coincide with the curve (13b) of the antenna having the largest period along the $\sin\theta$-axis. Evidently, this is the case for the antenna closest to the reference antenna, i.e., $|n| = 1$.[8]

Considering again the arbitrary geocast delivery zone around the coordinates (d^{sol}, θ^{sol}) as solution to (14a) and (14b), then $\sin\theta_1(d^{sol}) = \sin\theta_n(d^{sol}),\ \forall n \neq 0, 1$ is imposed by the latter. After inserting (13b) for antennas 1 and n, this expression becomes

$$\frac{k_n}{n} - k_1 = \Big(\Delta f_1 - \frac{\Delta f_n}{n}\Big)\frac{1}{c}\big[d^{sol} - d^{steer}\big]. \tag{16}$$

An angular recurrence of this solution exists only if the above statement is satisfied for a second pair of integers k''_n and k''_1. Noting that the right-hand side of (16) is invariant to the value of the integers k_n, k_1, k''_n, and k''_1, this occurs only when $\frac{k_n}{n} - k_1 = \frac{k''_n}{n} - k''_1$ is satisfied. By writing $k''_1 = k_1 \pm u$ and $k''_n = k_n + w_n$, with $u \in \mathbb{Z}_0^+,\ w_n \in \mathbb{Z}_0$, this condition reduces to $w_n = \pm nu$. Integers u and w_n that comply to this expression always exist and it is invariant to the frequency offsets Δf_n, such that angular recurrences of a geocast delivery zone cannot be mitigated through FDA frequency offset design. Substitution of these results in (13b) reveals that the closest recurrence of the solution (d^{sol}, θ^{sol}) to (14a) and (14b) is found for $u = 1$ at coordinates $(d^{sol}, \sin\theta^{sol} \pm \frac{\lambda_0}{b})$ in the $(d, \sin\theta)$-plane, leading to the following property.

Property 2 (Angular Periodicity)**.** *Angular recurrences of a geocast delivery zone for an FDA-SDF system with uniform antenna spacing b exist for any set of frequency offsets Δf_n. They are periodic with periodicity $T_{\sin\theta} = \frac{\lambda_0}{b}$ along the $\sin\theta$-axis.*

2) Geocast Delivery Zone(s) in Base Case: By Property 2, the $\sin\theta$ geocast delivery zone periodicity is equal to that of the residual phase condition solution (13b) for $|n| = 1$, i.e., having the largest $\sin\theta$ period. As such, identifying the geocast delivery zones and solutions to (14a) and (14b) located on the curve (13a) or (13b) for $n = 1$ and $k_1 = 0$ suffices to find all other geocast delivery zone locations through application of the periodicity properties from Section III-B1. From (14a) and (14b) one finds that such a solution satisfies $\sin\theta_1(d)|_{k_1=0} = \sin\theta_n(d),\ d_1(\theta)|_{k_1=0} = d_n(\theta),\ \forall n \neq 0, 1$. Substitution of, respectively, (13b) and (13a) in the above statements yields the following expressions for the coordinates that satisfy them

$$\begin{cases} d = d^{steer} + c\dfrac{k_n}{n\Delta f_1 - \Delta f_n} \\ \sin\theta = \sin\theta^{steer} + \dfrac{\lambda_0}{b}\dfrac{\Delta f_1 k_n}{n\Delta f_1 - \Delta f_n}. \end{cases} \tag{17}$$

A geocast delivery zone is established only if the above coordinates (17) coincide for all antennas $n \neq 0, 1$. Therefore, the

[8]For clarity, $n = 1$ is used in the following derivation. Identical results are obtained when considering $n = -1$, if applicable.

integers $k_n,\ \forall n \neq 0,1$ that characterize the sought solutions should satisfy the following system of $N-3$ equations

$$\begin{aligned}\frac{k_{-N_1}}{-N_1\Delta f_1 - \Delta f_{-N_1}} = \cdots = \frac{k_{-1}}{-\Delta f_1 - \Delta f_{-1}} \\ = \frac{k_2}{2\Delta f_1 - \Delta f_2} = \cdots = \frac{k_{N_2}}{N_2\Delta f_1 - \Delta f_{N_2}}.\end{aligned} \tag{18}$$

The above expression is a system of homogeneous linear Diophantine equations (HLDEs), each in 2 of the integer variables k_n [35]. In general, such a system is represented as $\frac{\kappa_1}{a_1} = \frac{\kappa_2}{a_2} = \cdots = \frac{\kappa_P}{a_P}$, $P \in \mathbb{N}_0$, with variables $\kappa_1, \kappa_2, \ldots, \kappa_P$, of which only integer solutions are of interest, and coefficients $a_1, a_2, \ldots, a_P$. The trivial solution $\kappa_1 = \kappa_2 = \cdots = \kappa_P = 0$ to this problem always exists. From [35], it can be proven that nontrivial integer solutions exist only when the coefficients $a_1, a_2, \ldots, a_P$ are integers. The solutions are then given by $\kappa_n = k\frac{a_n}{\gcd(a_1,\ldots,a_P)},\ k \in \mathbb{Z}$, where $\gcd(\mathcal{A})$ returns the greatest common divisor of the elements in the set $\mathcal{A}$. Applied to (18) for the two identified frequency offset categories, the above considerations yield the following results.

a) Rational Frequency Offsets: Given the definition of a rational frequency offset configuration, i.e., $\Delta f_n = \frac{p_n}{q}\Delta f_{\tilde{n}},\ \frac{p_n}{q} \in \mathbb{Q}$, the coefficients $n\Delta f_1 - \Delta f_n$ in the system (18) of HLDEs reduce to $np_1 - p_n$. The rational nature of the fractions $\frac{p_n}{q}$ implies that $p_n \in \mathbb{Z}$, such that these coefficients are integers. By the prior considerations on HLDEs, the system (18) then has nontrivial solutions that are given by

$$k_n = k\frac{np_1 - p_n}{\gcd\left(\{np_1 - p_n | n \neq 0,1\}\right)}, \quad k \in \mathbb{Z}. \tag{19}$$

Substitution of these results, together with the rational frequency offset definition, in the coordinates (17) shows that the geocast delivery zones on the curve (13b) for $n = 1$ and $k_1 = 0$ are located at the following coordinates

$$\begin{cases} d = d^{steer} + q\dfrac{c}{\Delta f_{\tilde{n}}}\dfrac{k}{D} \\ \sin\theta = \sin\theta^{steer} + \dfrac{\lambda_0}{b}\dfrac{p_1 k}{D}, \end{cases} \tag{20}$$

where $D = \gcd\left(\{np_1 - p_n | n \neq 0,1\}\right)$. These solutions can be remapped, using the periodicity Properties 1 and 2, to bound them to a single spatial period $d^{steer} \leq d < d^{steer} + T_d$, $\sin\theta^{steer} \leq \sin\theta < \sin\theta^{steer} + T_{\sin\theta}$, i.e., the base case. One finds

$$\begin{cases} d = d^{steer} + q\dfrac{c}{|\Delta f_{\tilde{n}}|}\dfrac{k'}{D} \\ \sin\theta = \sin\theta^{steer} + \dfrac{\lambda_0}{b}\dfrac{(p_1 k' \bmod D)}{D}, \end{cases} \tag{21}$$

where $k' = 0, 1, \ldots, D-1$, and $(\alpha \bmod \beta)$ is the modulo operator returning the remainder after division of α by β.

b) Irrational Frequency Offsets: Given the definition of an irrational frequency offset configuration, i.e., $\exists n : \Delta f_n = \rho_n \Delta f_{\tilde{n}},\ \rho_n \in \mathbb{R} \setminus \mathbb{Q}$, there exists at least one coefficient $n\Delta f_1 - \Delta f_n$ in the system (18) of HLDEs that is not an integer. Therefore, only the trivial solution $k_{-N_1} = \cdots = k_{-1} = k_2 = \cdots = k_{N_2} = 0$ exists. As a result, the only geocast delivery zone coinciding with the curve (13b) for $n = 1$ and $k_1 = 0$, and thus within the base case's single spatial period, is located at the target coordinates

$$\begin{cases} d = d^{steer} \\ \sin\theta = \sin\theta^{steer}. \end{cases} \tag{22}$$

3) Complete Set of Geocast Delivery Zone Locations: Applying the periodicity Properties 1 and 2 from Section III-B1 to the base case solutions from Section III-B2 allows to describe the geocast delivery zone positions in the entire $(d, \sin\theta)$-plane. By defining $k_d, k_\theta \in \mathbb{Z}$, one finds the following results.

a) Rational Frequency Offsets: From the base case solutions (21), all geocast delivery zone locations for an FDA-SDF system with rational frequency offsets are found. Their coordinates are given by

$$\begin{cases} d = d^{steer} + q\dfrac{c}{|\Delta f_{\tilde{n}}|}\left(\dfrac{k'}{D} + k_d\right) \\ \sin\theta = \sin\theta^{steer} + \dfrac{\lambda_0}{b}\left(\dfrac{(p_1 k' \bmod D)}{D} + k_\theta\right). \end{cases} \tag{23}$$

The above result should be interpreted as follows. The integer k' describes the position of a geocast delivery zone within the base case's single spatial period (or any periodic recurrence thereof). The integers k_d and k_θ indicate by how many periods, in the radial and azimuthal domain respectively, this solution is shifted with respect to its base case equivalent.

b) Irrational Frequency Offsets: The geocast delivery zone locations for an FDA-SDF system with irrational frequency offsets are found from the corresponding base case solution (22). They are located at the coordinates

$$\begin{cases} d = d^{steer} \\ \sin\theta = \sin\theta^{steer} + \dfrac{\lambda_0}{b}k_\theta. \end{cases} \tag{24}$$

Thus, as anticipated by Property 1, geocast delivery zones for irrational frequency offsets are unique in the radial domain, in contrast to the locations (23) for rational frequency offsets.

C. Geocast Delivery Zone Uniqueness

The solutions (23) and (24) to the perfect data retrieval conditions (14a) and (14b) confirm the presence of a geocast delivery zone at the desired target coordinates $(d^{steer}, \theta^{steer})$, for $k', k_d, k_\theta = 0$. However, solutions for $k', k_d, k_\theta \neq 0$ generate spurious zones of correct data retrieval at undesired positions and should thus be mitigated to ensure uniqueness of the intended geocast delivery zone.

1) Rational Frequency Offsets: Given the radial dimension's infinite character and the radially periodic nature of geocast delivery zone locations (23) for rational frequency offsets, radial uniqueness in this scenario cannot be guaranteed theoretically. However, in practice, a distance d^{lim} exists beyond which data recovery becomes impossible – either through excessive path loss and insufficient SNR or physical

obstructions constraining the receiver's position. Under this assumption, radial uniqueness is ensured when only the intended geocast delivery zone at the target coordinates $(d^{steer}, \theta^{steer})$ exists in the range $[0, d^{lim}]$. Using (23), this translates to the condition

$$\begin{cases} d^{steer} + q\dfrac{c}{|\Delta f_{\tilde{n}}|}\left(\dfrac{k'}{D} + k_d\right) < 0 & \dfrac{k'}{D} + k_d < 0 \\ d^{lim} < d^{steer} + q\dfrac{c}{|\Delta f_{\tilde{n}}|}\left(\dfrac{k'}{D} + k_d\right) & \dfrac{k'}{D} + k_d > 0. \end{cases} \tag{25}$$

Noting that $\left|\frac{k'}{D} + k_d\right| = \frac{1}{D}$ yields the strictest constraints, an upper bound is found on the smallest frequency offset $\Delta f_{\tilde{n}}$, guaranteeing radial uniqueness of an FDA-SDF geocast delivery zone for rational frequency offsets when

$$|\Delta f_{\tilde{n}}| < \frac{q}{D} \min\left\{\frac{c}{d^{steer}}, \frac{c}{d^{lim} - d^{steer}}\right\}. \tag{26}$$

Uniqueness in the azimuthal domain is ensured when all spurious geocast delivery zones are located at imaginary azimuthal coordinates $\theta \in \mathbb{C} \setminus \mathbb{R}$. By (23), this is satisfied when

$$\left|\sin\theta^{steer} + \frac{\lambda_0}{b}\left(\frac{k''}{D} + k_\theta\right)\right| > 1, \quad \forall k'', k_\theta \neq 0, \tag{27}$$

where $k'' = (p_1 k' \bmod D) = 0, 1, \ldots, D-1$. Again, the strictest constraint is obtained for $\left|\frac{k''}{D} + k_\theta\right| = \frac{1}{D}$. As such, azimuthal uniqueness of an FDA-SDF geocast delivery zone for rational frequency offsets is guaranteed when the antenna spacing b satisfies the upper bound

$$b < \frac{\lambda_0}{D}\frac{1}{1 + |\sin\theta^{steer}|}. \tag{28}$$

It should be noted that, in general, the uniqueness conditions (26) and (28) should not be satisfied simultaneously. Indeed, the integers k' and k'' are not independent. Therefore, stating that $\left|\frac{k'}{D} + k_d\right|$ or $\left|\frac{k''}{D} + k_\theta\right| = \frac{1}{D}$ in one of the conditions (25) or (27), fixes the value of, respectively, k'' and k' in the other, which is thus not necessarily in its strictest form. Intuitively, a spurious geocast delivery zone mitigated by satisfying the uniqueness condition for one dimension is no longer physically present and hence should not be considered when defining the uniqueness condition in the other dimension.

2) Irrational Frequency Offsets: By (24), the use of irrational frequency offsets guarantees radial geocast delivery zone uniqueness by design. Therefore, no additional restrictions apply to the frequency offsets Δf_n to guarantee radial uniqueness in this scenario.

An analogous reasoning to the rational frequency offset scenario easily shows that, for irrational frequency offsets, the upper bound on the antenna spacing b, guaranteeing azimuthal uniqueness of an FDA-SDF geocast delivery zone, becomes

$$b < \lambda_0 \frac{1}{1 + |\sin\theta^{steer}|}. \tag{29}$$

Upon comparison with (28), irrational frequency offsets are noted to allow wider antenna spacing than rational frequency offsets (and, by Section III-D below, higher azimuthal precision) without jeopardizing azimuthal uniqueness of the geocast delivery zone.

D. Geocast Delivery Zone Size

By the above, a unique geocast delivery zone is generated around the target coordinates $(d^{steer}, \theta^{steer})$. It is formally defined as the geographical area around these coordinates where the BER remains below a threshold P_e^{th} that ensures successful recovery of transmitted information. By defining the threshold phase Φ_{th} as the phase rotation at which the BER reaches the threshold P_e^{th}, the geocast delivery zone is described as the set of positions (d, θ) where the residual phase shift on the received symbols (9) is bounded by Φ_{th} for all antennas n. By introducing (11a), (11b), and (12) in the residual phase expression (left-hand side of (10)) and noting again that $\Delta f_n \ll f_c = f_0 \Rightarrow \frac{f_n}{c} \approx \frac{f_0}{c} = \frac{1}{\lambda_0}$, one finds the condition

$$\begin{aligned} -\Phi_{th} < 2\pi\frac{nb}{\lambda_0}\left[\sin\theta - \sin\theta^{steer}\right] \\ - 2\pi\frac{\Delta f_n}{c}\left[d - d^{steer}\right] < \Phi_{th}. \end{aligned} \tag{30}$$

By isolating $\sin\theta$ or d in (30), upper and lower bounds, respectively for the azimuthal and radial coordinates, are found for each antenna n that describe the spatial region where the corresponding received symbols are subject to sub-threshold residual phase distortion, and thus yield sub-threshold BER. They are given in (31a) and (31b) at the bottom of this page. The overall FDA-SDF BER is below the threshold only when the conditions (31a) and (31b) are satisfied for all antennas n, such that the geocast delivery zone corresponds to the area where these ranges overlap for all antennas n. Its edges are therefore established at the intersection of the lowest upper bound with the highest lower bound. By equaling the lower bound for an antenna $\check{n}$ and upper bound for an antenna $\hat{n}$ in (31a) and (31b), one finds, respectively, the radial and

$$\sin\theta^{steer} - \tfrac{\lambda_0}{|n|b}\tfrac{\Phi_{th}}{2\pi} + \mathrm{sgn}(n)\tfrac{\lambda_0}{|n|b}\tfrac{\Delta f_n}{c}\left[d - d^{steer}\right] < \sin\theta < \sin\theta^{steer} + \tfrac{\lambda_0}{|n|b}\tfrac{\Phi_{th}}{2\pi} + \mathrm{sgn}(n)\tfrac{\lambda_0}{|n|b}\tfrac{\Delta f_n}{c}\left[d - d^{steer}\right] \tag{31a}$$

$$d^{steer} - \tfrac{c}{|\Delta f_n|}\tfrac{\Phi_{th}}{2\pi} + \mathrm{sgn}(\Delta f_n)\tfrac{c}{|\Delta f_n|}\tfrac{nb}{\lambda_0}\left[\sin\theta - \sin\theta^{steer}\right] < d < d^{steer} + \tfrac{c}{|\Delta f_n|}\tfrac{\Phi_{th}}{2\pi} + \mathrm{sgn}(\Delta f_n)\tfrac{c}{|\Delta f_n|}\tfrac{nb}{\lambda_0}\left[\sin\theta - \sin\theta^{steer}\right] \tag{31b}$$

TABLE I
OVERVIEW OF ELEMENTARY FDA CONFIGURATIONS AND THEIR SPATIAL PROPERTIES FOR FDA-SDF

FDA Type	Frequency Offset Values, Δf_n	Uniqueness Conditions		Geocast-width	
		Radial*, $\lvert\Delta f_{\check{n}}\rvert <$	Angular, $b <$	Radial, $\lvert F_d(\check{n}_d,\hat{n}_d)\rvert$	Angular, $\lvert F_\theta(\check{n}_\theta,\hat{n}_\theta)\rvert$
symm. lin. [36]	$\lvert n\rvert\Delta f$ †	$\frac{1}{2}\frac{c}{d^{steer}}$	$\frac{1}{2}\frac{\lambda_0}{1+\lvert\sin\theta^{steer}\rvert}$	$\frac{2}{N-1}\frac{1}{\Delta f}$	$\frac{2}{N-1}$
altern. lin. [33]	$\begin{cases}+n\Delta f & n \text{ odd}\\ -n\Delta f & n \text{ even}\ ‡\end{cases}$	$\frac{1}{4}\frac{c}{d^{steer}}$	$\frac{1}{4}\frac{\lambda_0}{1+\lvert\sin\theta^{steer}\rvert}$	$\frac{2N-3}{2(N-1)(N-2)}\frac{1}{\Delta f}$	$\frac{2N-3}{2(N-1)(N-2)}$
symm. log. [37]	$\log_a(\lvert n\rvert+1)\Delta f$ †	n.a.	$\frac{\lambda_0}{1+\lvert\sin\theta^{steer}\rvert}$	$\log_a^{-1}\left(\frac{N+1}{2}\right)\frac{1}{\Delta f}$	$\frac{2}{N-1}$
altern. log.	$\begin{cases}+\log_a(n+1)\Delta f & n \text{ odd}\\ -\log_a(n+1)\Delta f & n \text{ even}\ ‡\end{cases}$	n.a.	$\frac{\lambda_0}{1+\lvert\sin\theta^{steer}\rvert}$	$\frac{2N-3}{\log_a\left(N^{N-2}(N-1)^{N-1}\right)}\frac{1}{\Delta f}$	$\log_{N^{N-2}(N-1)^{N-1}}\left(N(N-1)\right)$

* For simplicity, $d^{lim} < 2d^{steer}$ is assumed in (26)
† Central reference antenna: $n = -\frac{N-1}{2},\dots,\frac{N-1}{2}$
‡ Edge reference antenna: $n = 0, 1, \dots, N-1$

azimuthal coordinates of their intersection. They are given by

$$d = d^{steer} \pm c\underbrace{\frac{|\check{n}|+|\hat{n}|}{\mathrm{sgn}(\check{n})|\hat{n}|\Delta f_{\hat{n}}-\mathrm{sgn}(\hat{n})|\check{n}|\Delta f_{\hat{n}}}}_{F_d(\check{n},\hat{n})}\frac{\Phi_{th}}{2\pi}, \tag{32a}$$

$$\sin\theta = \sin\theta^{steer} \pm \frac{\lambda_0}{b}\underbrace{\frac{|\Delta f_{\hat{n}}|+|\Delta f_{\hat{n}}|}{\mathrm{sgn}(\Delta f_{\hat{n}})|\Delta f_{\hat{n}}|\check{n}-\mathrm{sgn}(\Delta f_{\hat{n}})|\Delta f_{\hat{n}}|\hat{n}}}_{F_\theta(\check{n},\hat{n})}\frac{\Phi_{th}}{2\pi}. \tag{32b}$$

The intersection of the lowest upper bound with the highest lower bound, which determines the geocast delivery zone size, then corresponds to the one having coordinates (32a) and (32b) closest to the respective target coordinates d^{steer} and θ^{steer}. In the radial domain, this is the case for antennas $\check{n}_d, \hat{n}_d = \arg\min_{\check{n},\hat{n}} |F_d(\check{n},\hat{n})|$; in the azimuthal domain, it is obtained for antennas $\check{n}_\theta, \hat{n}_\theta = \arg\min_{\check{n},\hat{n}} |F_\theta(\check{n},\hat{n})|$. The radial Θ_d and azimuthal Θ_θ width of the geocast delivery zone (i.e., geocast-width) are then given by the radial and angular range between the coordinates in (32a) and (32b) for the antennas $\check{n}_d, \hat{n}_d$ and $\check{n}_\theta, \hat{n}_\theta$, respectively. One finds

$$\Theta_d = 2c\left|F_d(\check{n}_d,\hat{n}_d)\right|\frac{\Phi_{th}}{2\pi}, \tag{33a}$$

$$\Theta_\theta = \mathrm{asin}\left(\sin\theta^{steer} + \frac{\lambda_0}{b}\left|F_\theta(\check{n}_\theta,\hat{n}_\theta)\right|\frac{\Phi_{th}}{2\pi}\right) - \mathrm{asin}\left(\sin\theta^{steer} - \frac{\lambda_0}{b}\left|F_\theta(\check{n}_\theta,\hat{n}_\theta)\right|\frac{\Phi_{th}}{2\pi}\right). \tag{33b}$$

The phase threshold Φ_{th} depends strongly on the communication scenario. A thorough examination of its characteristics is beyond the scope of this paper. However, analytical expressions for PSK and QAM constellations in a simple AWGN free space scenario are provided in Appendix A.

E. Discussion on Frequency Offset Configuration

It should be emphasized that the above analysis provides a deterministic and closed-form description of FDA-SDF's geographical properties and design rules for any arbitrary frequency offset arrangement. Nevertheless, this paper additionally proposes a novel alternating logarithmic frequency offset configuration that optimally exploits the derived properties. It logarithmically increases the absolute value of consecutive frequency offsets, while alternating their sign. More specifically,

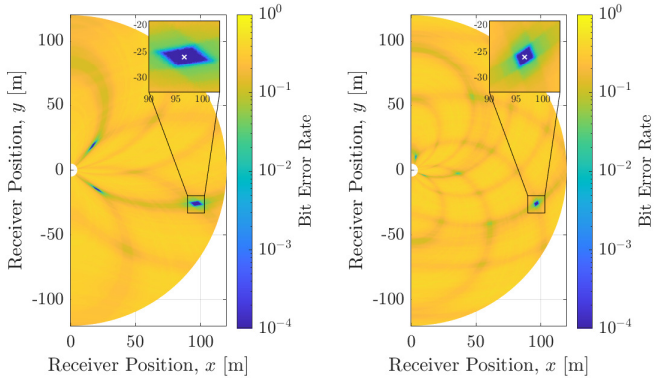

(a) Alternating linear FDA-SDF (b) Alternating logarithmic FDA-SDF

Fig. 2. Spatial BER distribution of FDA-SDF with $N = 4$ antennas. White $\times$ marks target position.

given a base frequency offset $\Delta f > 0$ and logarithm base $a > 1$, the n-th antenna's frequency offset is defined as

$$\Delta f_n = \begin{cases}+\log_a(n+1)\Delta f & n \text{ odd}\\ -\log_a(n+1)\Delta f & n \text{ even},\end{cases} \tag{34}$$

for $n = 0, 1, \dots, N-1$, i.e., a reference antenna at the array edge. The irrational frequency offset nature maximizes the geocast delivery zone's azimuthal uniqueness interval, while avoiding radial recurrence entirely. Additionally, the outermost reference antenna placement yields maximal values for the antenna index n, minimizing the parameter $\left|F_\theta(\check{n}_\theta,\hat{n}_\theta)\right|$ in (33b) and thus the azimuthal geocast delivery zone width, while the logarithm base a provides an additional degree of freedom to manipulate its radial width by controlling the frequency offset values in the parameter $\left|F_d(\check{n}_d,\hat{n}_d)\right|$ of (33a). This is illustrated in Table I, where the FDA-SDF spatial properties are derived for the proposed alternating logarithmic frequency offsets and compared to related configurations with symmetrical linear [36], alternating linear [33], and symmetrical logarithmic [37] frequency offsets. Further performance analyses of FDA-SDF in general and alternating logarithmic frequency offsets in particular are given in Section IV.

IV. SIMULATIONS AND PERFORMANCE EVALUATION

The following system parameters are used to simulate the proposed FDA-SDF scheme. The input symbol stream

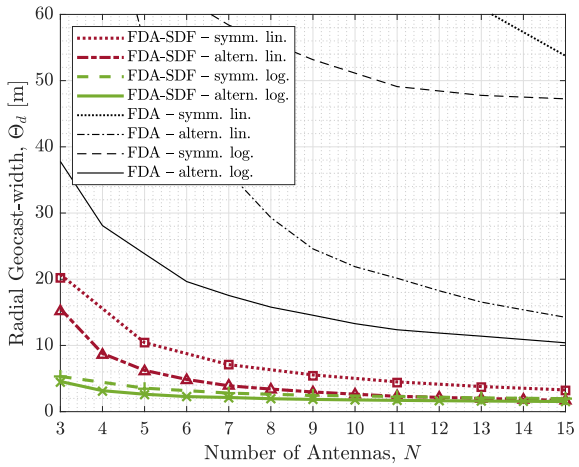

Fig. 3. Radial geocast delivery zone width, for varying number of antennas N. Markers represent theoretical predictions (33a) for each respective FDA-SDF frequency offset configuration.

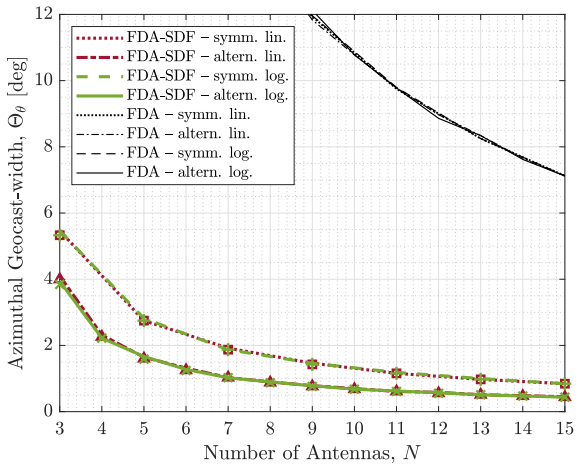

Fig. 4. Azimuthal geocast delivery zone width, for varying number of antennas N. Markers represent theoretical predictions (33b) for each respective FDA-SDF frequency offset configuration.

consists of 16-QAM symbols, mapped from an arbitrary bitstream of length 10^5 using traditional Gray coding. A target range and angle of, respectively, $d^{steer} = 100$ m and $\theta^{steer} = -15°$ are employed for steering phase configuration. Unless specified otherwise, the number of antennas N is varied, while the antenna spacing is fixed at $b = 0.75\lambda_0$, satisfying the azimuthal uniqueness condition (29) for the proposed alternating logarithmic frequency offsets. The base carrier frequency is set to $f_c = f_0 = 3.6$ GHz, for a symbol rate of $B = 50$ MHz. Frequency offsets are constructed as in Table I, using a base frequency offset $\Delta f = 1$ MHz and, where applicable, a logarithm base $a = 1.2$, which equalizes the radial precision of the alternating logarithmic and alternating linear configurations for the largest investigated array size of $N = 15$ antennas. The SNR is fixed to $\gamma_s = 25$ dB and an uncoded BER threshold of $P_e^{th} = 10^{-3}$ is used for geocast delivery zone characterization.

Fig. 2 compares the spatial BER distribution of FDA-SDF for alternating linear and alternating logarithmic frequency offsets, both using an array of $N = 4$ antennas along the y-axis and placed at the origin. In both scenarios, a geocast delivery zone of sub-threshold BER and thus correct data recovery is successfully generated around the target position. As anticipated in Section III-E, it is unique only in the latter scenario, whereas, by Table I, the former requires decreased antenna spacing or frequency offsets for sidelobe mitigation at the cost of increased geocast delivery zone size.[9] Nevertheless, despite the rudimentary nature of the employed frequency offset schemes, uniqueness conditions are straightforward whenever necessary and geocast delivery zones are isolated and well delineated. FDA-SDF therefore allows to significantly reduce overall design complexity compared to conventional beamforming FDA implementations that require complexified frequency offset design [14] or DM processing [16]–[19] to suppress sidelobes of increased power and decreased BER that otherwise spread out from the main lobe.

Evaluation of FDA-SDF's spatial focusing precision is done in Figs. 3 and 4, respectively showing the radial and azimuthal geocast-width for each of the frequency offset schemes in Table I. They are compared with their respective theoretical estimations (33a) and (33b), as well as with beamforming-based FDA using the same array and frequency offset configuration. The latter results are obtained by transmitting identical but phase-shifted symbols using the time-invariant FDA model proposed in Section II-A and recombining the received symbols (6) by summation, as in the SAMC FDA schemes [25], [26]. For a fair comparison, noise is added such that the target position's SNR is identical to the FDA-SDF scenario. At other positions, by [38], [39], the SNR's spatial variation impacts the BER accordingly, allowing to evaluate the beamforming-based FDA geocast delivery zone, of which the width is shown in Figs. 3 and 4, using the same BER threshold as for FDA-SDF.[10]

The results in Figs. 3 and 4 validate a good match of simulation observations and theoretical predictions of the FDA-SDF geocast-width and illustrate the degrees of freedom for its manipulation. That is, the dependency of radial precision on the frequency offset magnitude and distribution among the antennas (as illustrated by the different precision for each frequency offset scheme in Fig. 3) and the improvement of angular precision by displacement of the reference antenna $n = 0$ away from the array center (as exhibited by both alternating frequency offset schemes, outperforming their symmetrical counterparts in Fig. 4). Additionally, the logarithm-based frequency offset schemes exhibit a flattened radial precision evolution as a function

[9] Analogous observations can be made for symmetrical linear and symmetrical logarithmic frequency offsets, as apparent from Table I.

[10] Note that consideration of DM processing is omitted given the invalidation of FDA-DM's envisioned PLS benefits over conventional FDA and FDA-SDF, either by time-variance [20], [21] or common transmitter-receiver time-frames and cooperative receiver processing in [25], [26] and derivated works.

of array size (controlled by the logarithm base a), allowing them to achieve improved radial precision for smaller arrays, compared to their linear counterparts. As anticipated in Section III-E, the proposed alternating logarithmic frequency offset configuration combines all of the above precision benefits, together with optimal uniqueness conditions, making it an ideal choice for use in FDA-SDF applications. Additionally, note that, while beamforming-based FDA shares the frequency offset magnitude degree of freedom for radial precision manipulation (as apparent from Fig. 3), its azimuthal geocast-width in Fig. 4 is invariant to changes in the reference antenna position. As such, the latter is a novel degree of freedom, exclusive to FDA-SDF, that provides a low-cost and low-complexity opportunity for FDA azimuthal precision manipulation.

Most importantly, Figs. 3 and 4 show FDA-SDF's spatial precision superiority over beamforming-based FDA. Indeed, for any frequency offset configuration, the FDA-SDF geocast delivery zone is significantly smaller in both the radial and azimuthal dimensions than its FDA counterpart. In particular, while not visible in the figures, a 3-antenna FDA-SDF setup matches the radial and angular precision of its FDA counterpart using, respectively, 14 and 24 antennas for alternating linear frequency offsets, or 64 and 24 antennas for alternating logarithmic frequency offsets. The former results affirm the observations in [33]. The latter shows that conventional FDA's typically mid to large-scale arrays fail to exploit the flattened radial precision versus array size feature of the proposed alternating logarithmic frequency offset scheme, in contrast to FDA-SDF's small-scale arrays that optimally benefit from it.

V. Conclusion and Perspectives

In this paper, a novel unified frequency diverse array (FDA) and spatial data focusing (SDF) approach is proposed for wireless physical layer geocasting, i.e., spatially confined broadcasting. By combining SDF's high spatial focusing precision and FDA's flexible frequency offset design, it simultaneously overcomes large-scale array requirements of classical beamforming-based FDA and OFDM-SDF's limited degrees of freedom for geocast delivery zone manipulation. Additionally, SDF's inherent inter-antenna signal orthogonality and separate substream processing at the receiver are exploited to more efficiently implement a SAMC receiver architecture for time-invariant FDA.

A hybrid FDA-based SDF (FDA-SDF) system model is presented in free space. A comprehensive analytical derivation provides a deterministic and closed-form description of the proposed scheme's geographical properties and design rules, such as geocast delivery zone steering, location, uniqueness, and size. Additionally, although derivations are general for any arbitrary frequency offset configuration, novel alternating logarithmic frequency offsets are proposed that mitigate radial periodicity and maximize azimuthal separation of the geocast delivery zone, while minimizing its size.

Theoretical results are supported by a simulation-based analysis of the proposed scheme. It confirms FDA-SDF's ability to generate a unique and well delineated geocast delivery zone with minimal frequency offset complexity and array size. Most importantly, it demonstrates FDA-SDF's improved spatial precision over beamforming-based FDA. Using alternating logarithmic frequency offsets, a 3-antenna FDA-SDF setup is shown to match the radial and azimuthal precision of its beamforming-based FDA counterpart using, respectively, 64 and 24 antennas.

Appendix A
Residual Phase Threshold for AWGN Channels

In noiseless free space scenarios, the first SDF-induced symbol errors (i.e., occurring closest to the target position with the smallest residual phase shift) instantly push the BER above any meaningful threshold P_e^{th}. Then, the phase threshold Φ_{th} in the geocast-width expressions (33a) and (33b) corresponds to the smallest phase difference between any symbol in the constellation and its decision bounds. In [30], it is given for M-PSK and square M-QAM as, respectively,

$$\Phi_{th}^{PSK} = \frac{\pi}{M}, \tag{35}$$

$$\Phi_{th}^{QAM} = \frac{\pi}{4} - \operatorname{asin}\left(\frac{\sqrt{M}-2}{\sqrt{2}(\sqrt{M}-1)}\right). \tag{36}$$

The above decision bounds can be adjusted by a correction margin to account for noise in the channel, as shown below.

From [38], a high SNR approximation for the M-PSK bit error probability P_e^{PSK} over an AWGN channel for equiprobable Gray coded symbols at a phase margin Φ_m from their closest decision bound is found as

$$P_e^{PSK} \approx \frac{1}{\log_2 M} Q\left(\sqrt{2\gamma_s}\sin\Phi_m\right), \tag{37}$$

where $Q(\cdot)$ is the Q-function and $\gamma_s = \frac{E_s}{N_0}$ is the SNR per symbol for an average symbol energy E_s and noise power spectral density N_0. By isolating the phase margin Φ_m from (37) and subtracting it from the noiseless residual phase threshold (35), the corrected M-PSK residual phase threshold $\tilde{\Phi}_{th}^{PSK}$ for AWGN channels is found as

$$\tilde{\Phi}_{th}^{PSK} = \frac{\pi}{M} - \operatorname{asin}\left(\frac{1}{\sqrt{2\gamma_s}} Q^{-1}\left(\log_2(M) N P_e^{th}\right)\right), \tag{38}$$

where it was assumed that antennas with sub-threshold residual phase shifts have negligible impact on the global BER in SDF, i.e., $P_e^{th} = \frac{1}{N}\sum_n P_{e,n}^{PSK} \approx \frac{1}{N} P_e^{PSK}$.

Similarly, from [39], a high SNR approximation for the bit error probability P_e^{QAM} over an AWGN channel for equiprobable Gray coded square M-QAM symbols at a margin distance δ_m from their closest decision bound is found as

$$P_e^{QAM} \approx \frac{\sqrt{M}-1}{\sqrt{M}\log_2\sqrt{M}} Q\left(\frac{\delta_m}{\sqrt{N_0/2}}\right). \tag{39}$$

After isolating the margin distance δ_m from (39) and normalizing it by the decision bound distance $\delta = \sqrt{\frac{3E_s}{2(M-1)}}$ of an undistorted square M-QAM constellation, the normalized

margin distance δ_m/δ can be introduced in the noiseless phase threshold (36). As such, one finds that the corrected square M-QAM residual phase threshold $\tilde{\Phi}_{th}^{QAM}$ for AWGN channels is given by

$$\tilde{\Phi}_{th}^{QAM} = \frac{\pi}{4} - \operatorname{asin}\left(\frac{\sqrt{M}-2+\delta_m/\delta}{\sqrt{2}(\sqrt{M}-1)}\right), \tag{40}$$

with

$$\delta_m/\delta = \sqrt{\frac{M-1}{3\gamma_s}}Q^{-1}\left(\frac{\sqrt{M}\log_2\sqrt{M}}{\sqrt{M}-1}NP_e^{th}\right), \tag{41}$$

where the impact on the global SDF BER of antennas with sub-threshold residual phase shifts is again neglected, i.e., $P_e^{th} = \frac{1}{N}\sum_n P_{e,n}^{QAM} \approx \frac{1}{N}P_e^{QAM}$.

REFERENCES

[1] Q. Yu and G. Heijenk, "Abiding geocast for warning message dissemination in vehicular ad hoc networks," in *ICC Workshops - 2008 IEEE International Conference on Communications Workshops*, Beijing, China, May 2008, pp. 400–404.

[2] L. R. Gallego-Tercero, R. Menchaca-Mendez, M. E. Rivero-Angeles, and R. Menchaca-Mendez, "Efficient time-stable geocast routing in delay-tolerant vehicular ad-hoc networks," *IEEE Access*, vol. 8, pp. 171 034–171 048, Sep. 2020.

[3] I. Stojmenovic, "Position-based routing in ad hoc networks," *IEEE Communications Magazine*, vol. 40, no. 7, pp. 128–134, Jul. 2002.

[4] C. Maihofer, "A survey of geocast routing protocols," *IEEE Communications Surveys & Tutorials*, vol. 6, no. 2, pp. 32–42, Second Quarter 2004.

[5] N. Sidiropoulos, T. Davidson, and Z.-Q. Luo, "Transmit beamforming for physical-layer multicasting," *IEEE Transactions on Signal Processing*, vol. 54, no. 6, pp. 2239–2251, Jun. 2006.

[6] Y. Zhang, H.-M. Wang, Z. Ding, and M. H. Lee, "Non-orthogonal multiple access assisted multi-region geocast," *IEEE Access*, vol. 6, pp. 2340–2355, Dec. 2018.

[7] C. A. Balanis, *Antenna Theory: analysis and design*, 4th ed. Hoboken, NJ, USA: John Wiley & Sons, Inc., 2016, ch. 6, pp. 285–384.

[8] W.-Q. Wang, "Overview of frequency diverse array in radar and navigation applications," *IET Radar, Sonar & Navigation*, vol. 10, no. 6, pp. 1001–1012, Jul. 2016.

[9] C. Wang, J. Xu, G. Liao, X. Xu, and Y. Zhang, "A range ambiguity resolution approach for high-resolution and wide-swath SAR imaging using frequency diverse array," *IEEE Journal of Selected Topics in Signal Processing*, vol. 11, no. 2, pp. 336–346, Mar. 2017.

[10] S. Y. Nusenu and A. Basit, "Frequency diverse array antennas: From their origin to their application in wireless communication systems," *Journal of Computer Networks and Communications*, vol. 2018, May 2018.

[11] P. Antonik, M. Wicks, H. Griffiths, and C. Baker, "Frequency diverse array radars," in *2006 IEEE Conference on Radar*, Verona, NY, USA, Apr. 2006, pp. 215–217.

[12] W. Khan, I. M. Qureshi, and S. Saeed, "Frequency diverse array radar with logarithmically increasing frequency offset," *IEEE Antennas and Wireless Propagation Letters*, vol. 14, pp. 499–502, 2015.

[13] A. Basit, I. M. Qureshi, W. Khan, S. U. Rehman, and M. M. Khan, "Beam pattern synthesis for an FDA radar with hamming window-based nonuniform frequency offset," *IEEE Antennas and Wireless Propagation Letters*, vol. 16, pp. 2283–2286, 2017.

[14] Y. Liu, H. Ruan, L. Wang, and A. Nehorai, "The random frequency diverse array: A new antenna structure for uncoupled direction-range indication in active sensing," *IEEE Journal of Selected Topics in Signal Processing*, vol. 11, no. 2, pp. 295–308, Mar. 2017.

[15] M. P. Daly and J. T. Bernhard, "Directional modulation technique for phased arrays," *IEEE Transactions on Antennas and Propagation*, vol. 57, no. 9, pp. 2633–2640, Sep. 2009.

[16] J. Hu, S. Yan, F. Shu, J. Wang, J. Li, and Y. Zhang, "Artificial-noise-aided secure transmission with directional modulation based on random frequency diverse arrays," *IEEE Access*, vol. 5, pp. 1658–1667, 2017.

[17] B. Qiu, J. Xie, L. Wang, and Y. Wang, "Artificial-noise-aided secure transmission for proximal legitimate user and eavesdropper based on frequency diverse arrays," *IEEE Access*, vol. 6, pp. 52 531–52 543, 2018.

[18] J. Xie, B. Qiu, Q. Wang, and J. Qu, "Broadcasting directional modulation based on random frequency diverse array," *Wireless Communications and Mobile Computing*, vol. 2019, May 2019.

[19] B. Qiu, M. Tao, L. Wang, J. Xie, and Y. Wang, "Multi-beam directional modulation synthesis scheme based on frequency diverse array," *IEEE Transactions on Information Forensics and Security*, vol. 14, no. 10, pp. 2593–2606, Oct. 2019.

[20] K. Chen, S. Yang, Y. Chen, and S.-W. Qu, "Accurate models of time-invariant beampatterns for frequency diverse arrays," *IEEE Transactions on Antennas and Propagation*, vol. 67, no. 5, pp. 3022–3029, May 2019.

[21] Y. Ding, A. Narbudowicz, and G. Goussetis, "Physical limitation of range-domain secrecy using frequency diverse arrays," *IEEE Access*, vol. 8, pp. 63 302–63 309, Mar. 2020.

[22] Y. Xu and J. Xu, "Corrections to "Range-angle-dependent beamforming of pulsed-frequency diverse array" [jul 15 3262-3267]," *IEEE Transactions on Antennas and Propagation*, vol. 66, no. 11, pp. 6466–6468, Nov. 2018.

[23] R. Gui, W.-Q. Wang, C. Cui, and H. C. So, "Coherent pulsed-FDA radar receiver design with time-variance consideration: SINR and CRB analysis," *IEEE Transactions on Signal Processing*, vol. 66, no. 1, pp. 200–214, Jan. 2018.

[24] M. Tan, C. Wang, and Z. Li, "Correction analysis of frequency diverse array radar about time," *IEEE Transactions on Antennas and Propagation*, vol. 69, no. 2, pp. 834–847, Feb. 2021.

[25] S. Ji, W.-Q. Wang, H. Chen, and S. Zhang, "On physical-layer security of FDA communications over rayleigh fading channels," *IEEE Transactions on Cognitive Communications and Networking*, vol. 5, no. 3, pp. 476–490, Mar. 2019.

[26] S. Ke, M. He, X. Bu, and W. Cai, "A leakage-based directional modulation scheme for frequency diverse array in robot swarm networks," *IEEE Access*, vol. 8, pp. 107 823–107 837, Jun. 2020.

[27] J. Sarrazin, M. Odhiambo, S. Golstein, P. De Doncker, and F. Horlin, "Spatial data focusing: An alternative to beamforming for geocasting scenarios," in *2018 USNC-URSI Radio Science Meeting (Joint with AP-S Symposium)*, Boston, MA, USA, Jul. 2018, pp. 139–140.

[28] G. Molineaux, S. Golstein, M. Odhiambo, F. Horlin, P. De Doncker, and J. Sarrazin, "Spatial data focusing using time and IQ resources for wireless geocasting," in *2019 IEEE Global Communications Conference (GLOBECOM)*, Waikoloa, HI, USA, Dec. 2019.

[29] G. Molineaux, M. Odhiambo, F. Horlin, P. De Doncker, and J. Sarrazin, "OFDM-based spatial data focusing for high resolution 2-dimensional wireless geocasting," in *2020 IEEE 31st Annual International Symposium on Personal, Indoor and Mobile Radio Communications*, London, United Kingdom (Great Britain), Aug. 2020, pp. 1–6.

[30] G. Molineaux, F. Horlin, P. De Doncker, and J. Sarrazin, "OFDM-based spatial data focusing for wireless physical layer geocasting in multipath channels," *IEEE Transactions on Wireless Communications*, vol. 21, no. 7, pp. 5064–5074, Jul. 2022.

[31] F. Shu, X. Wu, J. Hu, J. Li, R. Chen, and J. Wang, "Secure and precise wireless transmission for random-subcarrier-selection-based directional modulation transmit antenna array," *IEEE Journal on Selected Areas in Communications*, vol. 36, no. 4, pp. 890–904, Apr. 2018.

[32] T. Shen, S. Zhang, R. Chen, J. Wang, J. Hu, F. Shu, and J. Wang, "Two practical random-subcarrier-selection methods for secure precise wireless transmissions," *IEEE Transactions on Vehicular Technology*, vol. 68, no. 9, pp. 9018–9028, Sep. 2019.

[33] G. Molineaux, F. Horlin, P. De Doncker, and J. Sarrazin, "Frequency diverse array spatial data focusing for high precision range-angle-based geocasting," in *2022 IEEE Global Communications Conference (GLOBECOM)*, Rio de Janeiro, Brazil, Dec. 2022.

[34] A. Goldsmith, "Zero Forcing (ZF) Equalizers," in *Wireless Communications*, 1st ed. Cambridge, United Kingdom: Cambridge University Press, 2005, ch. 11.4.1, pp. 333–334.

[35] H. Cohen, "Diophantine Equations of Degree 1," in *Number Theory – Volume I: Tools and Diophantine Equations*, 1st ed. New York, NY, USA: Springer, 2007, ch. 6.2, pp. 339–341.

[36] W.-Q. Wang, "DM using FDA antenna for secure transmission," *IET Microwaves, Antennas & Propagation*, vol. 11, no. 3, pp. 336–345, Feb. 2017.

[37] Y. Liao, W.-Q. Wang, and Z. Zheng, "Frequency diverse array beampattern synthesis using symmetrical logarithmic frequency offsets for target indication," *IEEE Transactions on Antennas and Propagation*, vol. 67, no. 5, pp. 3505–3509, May 2019.

[38] J. Lu, K. Letaief, J.-I. Chuang, and M. Liou, "M-PSK and M-QAM BER computation using signal-space concepts," *IEEE Transactions on Communications*, vol. 47, no. 2, pp. 181–184, Feb. 1999.

[39] K. Cho and D. Yoon, "On the general BER expression of one- and two-dimensional amplitude modulations," *IEEE Transactions on Communications*, vol. 50, no. 7, pp. 1074–1080, Jul. 2002.

Guylian Molineaux received the M.Sc. degree in Electrical Engineering from Vrije Universiteit Brussel (VUB), Belgium, in 2019, the Ph.D. degree in Engineering and Technology from Université Libre de Bruxelles (ULB), Belgium, in 2023, and the Ph.D. degree in Information and Communication Technology from Sorbonne Université (SU), France, in 2023. From 2019 to 2023, he was a FRIA Ph.D. Fellow of the Belgian Fonds de la Recherche Scientifique – FNRS, working in the OPERA – Wireless Communications Group of ULB and the Group of Electrical Engineering of Paris (GeePs) at SU. His Ph.D. research is based around wireless physical-layer geocasting, using Spatial Data Focusing.

François Horlin received the Ph.D. degree from the Université catholique de Louvain (UCL) in 2002. He specialized in the field of signal processing for digital communications. His Ph.D. research aimed at optimizing the multi-access for 3G cellular communications. He joined the Inter-university Micro-Electronics Center (IMEC) in 2006 as a senior scientist. He worked on the design of efficient transceivers that can cope with the channel and hardware impairments in the context of 4G cellular systems. In 2007, François Horlin became professor at the Université libre de Bruxelles (ULB). He is supervising a research team working on modern communication, localisation and passive radar systems.

Philippe De Doncker received the M.Sc. degree in Physics Engineering and the Ph.D. degree in science engineering from the Université libre de Bruxelles (ULB), Brussels, Belgium, in 1996 and 2001, respectively. He founded the Wireless Communications Group in 2007. He is currently a Full Professor with ULB, and leads the research activities on wireless channel modeling and electromagnetics.

Julien Sarrazin received his Engineering diploma/Master of Research, and Ph.D. degrees from the University of Nantes in France, in 2005 and 2008 respectively. In 2009 and 2010, he worked at the BK Birla Institute of Technology of Pilani, in India, where he was in charge of telecommunication-related teaching. In 2011 and 2012, he was a research engineer at Telecom ParisTech in Paris. Since September 2012, he is an Associate Professor at Sorbonne Université (formerly University of Pierre and Marie Curie) in Paris, where he is currently working in the GeePs research institute (Group of Electrical Engineering of Paris) in the field of Spatial Data Focusing, antenna design, and localization. His research interests also include channel modeling and physical layer security.